Calibration of a modified hardening soil model for kakiritic rocks

Étalonnage d'un modèle modifié d'écrouissage des sols pour les roches kakiritiques

Dong W., Anagnostou G.
ETH Zurich, Switzerland

ABSTRACT: The response of weak rocks to tunnel excavation is usually analysed by assuming that the ground behaves as a linearly elastic, perfectly plastic material obeying the Mohr-Coulomb yield criterion. This model fails, however, to map the non-linear stress-strain behavior and the stress dependency of stiffness observed in triaxial testing on typical weak tectonized rocks such as kakirites. As a consequence, an equivalent Young's modulus has to be adopted, which may prove to be a difficult task. The present paper shows that a modified hardening soil model, whose parameters can be determined by common triaxial tests, describes the behavior observed under triaxial testing conditions better than the Mohr-Coulomb model under different stress levels. It also eliminates the need for more or less arbitrary assumptions concerning the Young's modulus.

RÉSUMÉ : Lors de la conception, la réaction de la roche à l'excavation du tunnel en terrain tendre est généralement analysée en assumant un comportement élastique linéaire, parfaitement plastique du matériau en utilisant le critère de plasticité de Mohr-Coulomb. Cependant, ce modèle ne permet pas la description du comportement contrainte-déformation non-linéaire ainsi que la dépendance de la rigidité à l'égard des contraintes observées dans les essais triaxiaux sur des roches tendres tectonisées comme les kakirites. Par conséquent, le module d'Young équivalent doit être appliqué, ce qui peut, en fonction du degré de la non-linéarité actuelle et de la variation de la contrainte de confinement, se révéler être une tâche difficile. Le présent document montre qu'un modèle modifié d'écrouissage des sols, dont les paramètres peuvent être déterminés par des essais triaxiaux courants, décrit mieux le comportement observé sous différents niveaux de contraintes dans des conditions de test triaxial qu'avec le modèle de Mohr-Coulomb. Ce modèle élimine également le besoin de hypothèses plus ou moins arbitraires concernant le module d'Young. (roches poussantes, modèle modifié d'écrouissage des sols, dépendance de la rigidité à l'égard des contraintes.)

KEYWORDS: squeezing ground, modified hardening soil model, stress dependent stiffness

1 INTRODUCTION

The relationship between rock pressure and displacement of the excavation boundary is important for tunnel design particularly under so-called squeezing conditions (Kovári 1998). Considerable uncertainties persist with respect to quantifying this relationship, because it depends essentially on the constitutive behavior of the ground. The latter is usually considered as a homogeneous, isotropic, linearly elastic and perfectly plastic material obeying the Mohr-Coulomb yield criterion. This model (hereafter referred to as "MC model") is widely used in engineering practice, because it accounts for some important aspects of actual ground behavior, is relatively simple and contains a small number of easily identifiable and familiar parameters. However, the MC model cannot map some features of the rock behavior observed in triaxial tests. More specifically, triaxial tests on kakirite samples (a typical squeezing rock from the Alps) show that the stress-strain behavior is pronouncedly nonlinear and inelastic right from the start of deviatoric loading, while the MC model exhibits linear elastic behavior before yielding. Another drawback of the MC model is that it cannot map the observed stress dependency of stiffness. Applying the modulus determined at some stress levels to other stress levels may lead to inaccurate predictions. Due to the linearity of the MC model, an equivalent Young's modulus has to be adopted, which – besides being theoretically questionable – may (depending on the degree of the actual non-linearity and confining stress variety) prove to be a difficult task.

The present paper investigates whether an alternative constitutive model can better map the observed behavior under triaxial conditions. The considered model represents a slight modification of the well-known Hardening Soil model ("HS model") of the PLAXIS finite element code and will be referred to hereafter as the "Modified Hardening Soil" model ("MHS model"). Section 2 of the present paper introduces the model, while Section 3 determines the model parameters using the results of laboratory tests on kakiritic samples. Finally, the capability of the MHS model is discussed by comparing it with the MC model under triaxial drained shear conditions and different confining pressures (Section 4).

2 MODIFIED HARDENING SOIL MODEL

The detailed description of the original HS model can be found at Brinkgreve and Vermeer (1997). Benz et al. (2008) extended the original model by formulating the yield function in terms of the Lode angle. This makes it possible to replace the original Mohr-Coulomb yield surface easily by alternative failure criteria such as the Matsuoka-Nakai criterion, which considers the effect of the intermediate stress, does not exhibit singularities and simplifies, therefore, the numerical implementation.

The MHS model is slightly different from the HS model with respect, (i), to the dependency of the yield surface on the Lode angle, (ii), to the dilatancy law and, (iii), to the cap hardening part, which is not taken into account in the present model. The present Section outlines the formulation of the MHS model under triaxial test conditions. All stresses hereafter are effective stresses. Compressive stresses are taken as positive.

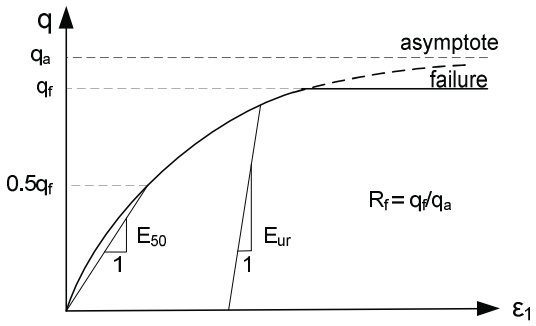

Figure 1. Hyperbolic stress-strain relationship in a CD triaxial test.

The MHS model is formulated within the framework of elasto-plasticity; the axial strain ε_1 is divided into an elastic part and a plastic part:

$$\varepsilon_1 = \varepsilon_1^e + \varepsilon_1^p \tag{1}$$

The elastic part of the axial strain depends linearly on the deviatoric stress q (Fig. 1).:

$$\varepsilon_1^e = \frac{q}{E_{ur}} \tag{2}$$

where E_{ur} denotes the elastic unloading-reloading modulus. The latter depends in general on the minimum principal stress σ_3 according to the following power law:

$$E_{ur} = E_{ur,ref}\left(\frac{\sigma_3 + c_f \cot\varphi_f}{p_{ref} + c_f \cot\varphi_f}\right)^m, \tag{3}$$

where $E_{ur,ref}$, c_f and φ_f denote the modulus at a reference pressure p_{ref}, the final cohesion and the final friction angle, respectively. The two shear strength parameters are identical with the cohesion and the friction angle of the standard MC model.

The MHS model adopts the basic idea of the HS model, which is to formulate the plastic part of the axial strain in such a way, that the overall response during primary loading in drained triaxial tests fulfills Duncan and Chang's (1970) hyperbolic relationship:

$$\varepsilon_1 = \frac{q}{2E_{50}}\frac{1}{1 - q/q_a} \quad \text{for } q < q_f, \tag{4}$$

where q_a and q_f denote the asymptotic deviatoric stress and the deviatoric stress at failure, respectively (Fig. 1). The latter is usually taken equal to a fraction of the asymptotic stress (i.e., $q_f = R_f\, q_a$, where R_f is a constant). E_{50} is the secant stiffness in primary loading at $q = 0.5\ q_f$ and depends on the minimum principal stress σ_3 via the same power law as the unloading-reloading modulus does:

$$E_{50} = E_{50,ref}\left(\frac{\sigma_3 + c_f \cot\varphi_f}{p_{ref} + c_f \cot\varphi_f}\right)^m = \frac{E_{50,ref}}{E_{ur,ref}} E_{ur}\,. \tag{5}$$

From Eqs (1), (2) and (4) we obtain the following relationship between the deviatoric stress and the plastic axial strain:

$$\frac{q}{2E_{50}}\frac{1}{1 - q/q_a} - \frac{q}{E_{ur}} - \varepsilon_1^p = 0\,. \tag{6}$$

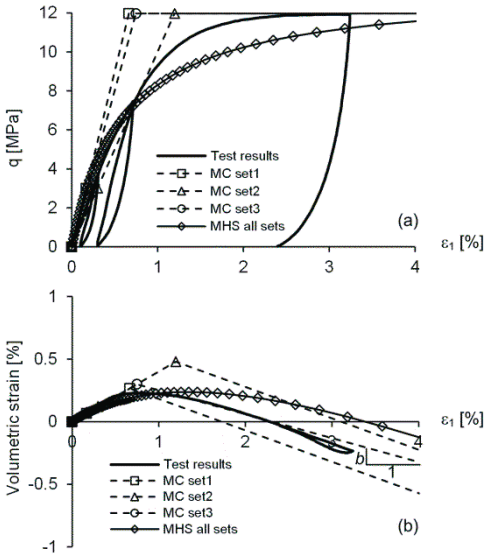

Figure 2. (a) Deviatoric stress and, (b), volumetric strain as a function of axial strain under a radial stress of 5 MPa (parameters: Table 1)

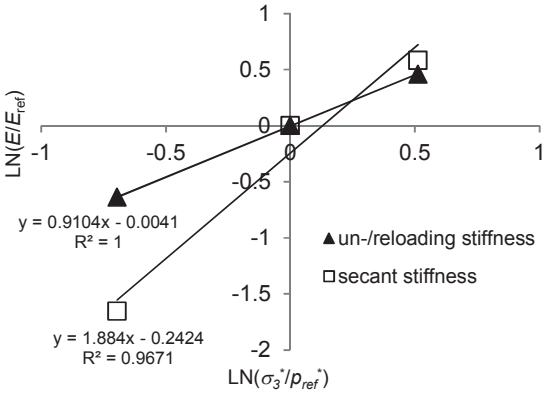

Figure 3. Relationship between E/E_{ref} and σ_3^*/p_{ref}^* in a log-log scale

Since the material is continuously yielding during primary loading, the left-hand-side of Eq. (6) represents the yield function:

$$f(\sigma, \gamma_s^{ps}) = \frac{q}{2E_{50}}\frac{1}{1 - q/q_a} - \frac{q}{E_{ur}} - \frac{2}{3}\gamma_s^{ps}\,. \tag{7}$$

This formulation contains as hardening parameter the plastic shear strain γ_s^{ps} instead of the plastic axial strain ε_1^p. This substitution is possible provided that the plastic volume changes are relatively small ($\gamma_s^{ps} = \varepsilon_1^p - \varepsilon_3^p = 1.5\,\varepsilon_1^p - 0.5\,\varepsilon_{vol}^p \cong 1.5\,\varepsilon_1^p$).

During hardening, the mobilized shear strength parameters increase from zero to their final values. The yield function (Eq. 7) can be written in terms of the mobilized friction angle φ_m. In order to reduce mathematical formalism, we apply Caquot's (1934) transformation to the normal stresses and formulate the yield condition and plastic potential in terms of the transformed average and deviatoric stresses, which reads as follows:

$$p^* = (\sigma_1^* + 2\sigma_3^*)/3 = p + c_f \cot\varphi_f \tag{8}$$

$$q^* = \sigma_1^* - \sigma_3^* = q\,. \tag{9}$$

During yielding the stresses fulfill the Mohr-Coulomb criterion with the mobilized friction angle φ_m (Eq. 10). At failure, q reaches q_f and φ_m reaches φ_f in Eq. (10).

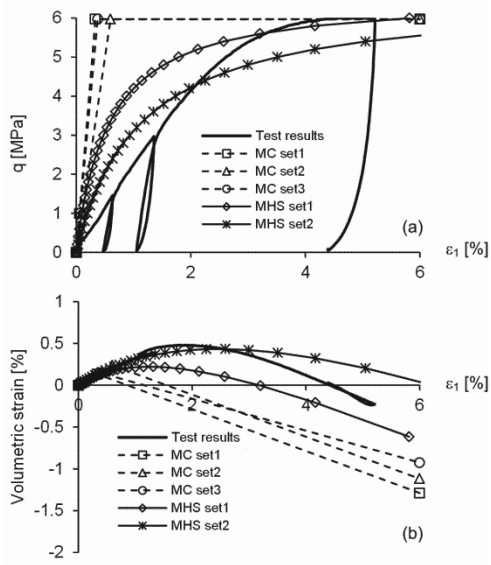

Figure 4. (a) Deviatoric stress and, (b), volumetric strain as a function of axial strain under a radial stress of 2 MPa (parameters: Table 1)

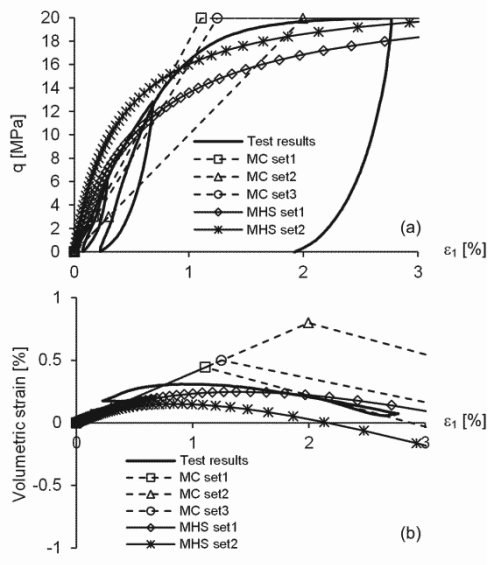

Figure 5. (a) Deviatoric stress and, (b), volumetric strain as a function of axial strain under a radial stress of 9 MPa (parameters: Table 1)

$$q^* = q = \frac{2\sin\varphi_m}{1-\sin\varphi_m}\sigma_3^* . \tag{10}$$

Substituting Eq. (10) into Eq. (7) and considering that $q_f = R_f\, q_a$ leads to Benz et al.'s (2008) formulation of the yield function:

$$f(\sigma,\gamma_s^{ps}) = \frac{3}{4}\frac{q^*}{E_{50}}\frac{1}{1-R_f\dfrac{1-\sin\varphi_f}{\sin\varphi_f}\dfrac{\sin\varphi_m}{1-\sin\varphi_m}} - \frac{3}{2}\frac{q^*}{E_{ur}} - \gamma_s^{ps} , \tag{11}$$

As mentioned by Benz et al. (2008), Eq. (11) is not limited to the Mohr-Coulomb failure criterion. In order to consider the effect of intermediate stress and simplify the numerical implementation they adopted the smooth Matsuoka-Nakai yield surface:

$$I_1^* I_2^* (1-\sin^2\varphi_m) - I_3^* (9-\sin^2\varphi_m) = 0 , \tag{12}$$

where I_1*, I_2* and I_3* are the transformed stress invariants. Based on this equation, the mobilized friction angle can be expressed in terms of the stress invariants and inserted into Eq. (11), which leads to the yield function of the MHS model for the Matsuoka-Nakai criterion.

The adopted flow rule is non-associated and corresponds to the cone-shaped plastic potential Drucker-Prager function:

$$\psi(\sigma) = q^* - p^* \frac{6\sin\psi_m}{3-\sin\psi_m} , \tag{13}$$

where ψ_m denotes the mobilized dilatancy angle. The original HS model assumed Rowe's (1962) dilatancy law, which, however, greatly overestimates the contractant behavior at low mobilized friction angles (Benz 2008). The MHS model adopts the relation of Soreide (1990):

$$\sin\psi_m = \left(\frac{\sin\varphi_m - \sin\varphi_{cs}}{1-\sin\varphi_m\sin\varphi_{cs}}\right)\left(\frac{\sin\varphi_m}{\sin\varphi_f}\right), \tag{14}$$

where φ_{cs} is the so-called critical mobilized friction angle. This parameter marks the boundary between contractant and dilatant behavior.

If the mobilized friction angle is lower than the critical mobilized friction angle, the mobilized dilatancy angle is negative, which means that the behavior is contractant. Otherwise the behavior is dilatant. The critical mobilized friction angle depends on the final values of the friction and dilatancy angles:

$$\sin\varphi_{cs} = \frac{\sin\varphi_f - \sin\psi_f}{1-\sin\varphi_f\sin\psi_f} . \tag{15}$$

As mentioned above, the MHS model does not include the cap hardening part of Benz's (2008) HS model. Under the conditions prevailing in triaxial tests as well as in the ground around deep tunnels, the stress path corresponds to mainly deviatoric shearing. The behavior can be solely simulated by the deviatoric hardening part, i.e. without considering cap hardening. In the absence of the latter, the parameters can be determined using conventional triaxial tests (no oedometric or isotropic compression tests needed) and the numerical implementation is simplified.

Table 1. Parameter values

MC model	Parameters	Set 1	Set 2	Set 3
	E [MPa]	1800	1000	1600
	ψ [°]	6.4	6.4	5
	Other parameters: $\nu = 0.3$, $c = 0.569$ MPa, $\varphi = 30°$			
MHS model	Parameter	Set 1	Set 2	
	m	0.91	1.88	
	Other parameters: $E_{ur,ref} = 1800$ MPa, $E_{50,ref} = 1152$ MPa, $p_{ref} = 5$ MPa, $\nu = 0.3$, $c_f = 0.569$ MPa, $\varphi_f = 30°$, $\psi = 6.4°$, $R_f = 0.9$			

The MHS model has a total of nine parameters, four of them ($E_{ur,ref}$, $E_{50,ref}$, p_{ref}, m) are used to determine the moduli E_{ur} and E_{50}. Another 4 parameters are same as in the Mohr-Coulomb model (ν, c_f, φ_f and ψ_f). The last parameter R_f, which defines the ratio between q_f and q_a, is usually taken equal to 0.9. As with the MC model, all the parameters have a clear physical meaning and can be determined using conventional triaxial tests.

3 PARAMETER IDENTIFICATION

The calibration of the model parameters is illustrated by considering the example of a typical kakirite sample taken from the Sedrun section of Gotthard Base Tunnel (Anagnostou et al. 2008). The sample was subjected to a multistage consolidated drained test (CD test) under consolidation pressures of 2, 5 and 9 MPa. The solid lines in Figures 2a and 2b show the deviatoric stress and the volumetric strain, respectively, as a function of the axial strain for a confining pressure of 5 MPa. The non-linearity of the stress-strain relationship before failure is significant. The unloading curves in Figure 2a show that irreversible strains develop right from the start of deviatoric loading.

The shear strength parameters of the MC model can be determined in the usual manner, i.e. from the regression line in the principal stress diagram. The dilatancy angle ψ of the MC model can be determined from the slope of the ε_1 and ε_{vol} curve (Fig. 2b), taking into account that the slope, i.e.

$$b = \frac{2\sin\psi}{1-\sin\psi}. \tag{16}$$

Three parameter sets were chosen for the MC model, which are different with respect to the Young's modulus and the dilatancy angle (Table 1). Parameter set 1 assumes that the Young's modulus is equal to the unloading-reloading modulus. Set 2 adopts the secant modulus as Young's modulus in order to better map the stress curve. Set 3 is slightly different from set 1 and was chosen in order to better map the volumetric strain behavior (Fig. 2). Poisson's ratio, which typically is in the range 0.20-0.35, was taken equal to 0.30.

The MHS model has, as mentioned in Section 2, nine parameters, four of which are the same as for the MC model (ν, c_f, φ_f and ψ_f). The reference mean stress p_{ref} is chosen as 5 MPa, which means that the moduli $E_{ur,ref}$ and $E_{50,ref}$ were determined under a radial stress of 5 MPa. The parameter m of the power law that expresses the stress dependency of the moduli (Eqs. 3 and 5) can be determined from the slope of the (E/E_{ref}) over (σ_3^*/p_{ref}^*) regression line in a log-log diagram (Fig. 3). According to Figure 3, m is equal to about 0.9 or 1.9 depending on the considered modulus (unloading-reloading or secant). In order to consider the influence of m, both parameter sets will be considered in the computations of the next Section.

4 MODEL BEHAVIOR IN TRIAXIAL DRAINED TESTS

The dashed lines in Figure 2 show the behavior of the MC model for the three-parameter sets of Table 1. Parameter set 1 overestimates the stress before failure. Set 2 better predicts the stress before failure, but cannot reproduce the unloading-reloading behavior satisfactorily, of course. In addition, as yielding occurs at a larger axial strain, the reversal in the volumetric behavior occurs also later in the case of set 2. Set 3 was chosen in order to map the volumetric strain behavior better. It presents of course the same problem as set 1 (overestimation of the pre-failure stress or, equivalently, underestimation of the pre-failure strain for given axial stress).

The behavior of the MHS model (solid line with points in Figure 2) can be easily determined by stepwise integrating the constitutive equations in a spreadsheet. The line applies to both parameter sets: As the radial stress is kept constant during deviatoric loading, the moduli E_{ur} and E_{50} remain constant and, since in the test of Figure 2 the radial stress is equal to the reference stress (5 MPa), $E_{ur} = E_{ur,ref}$, $E_{50} = E_{50,ref}$ and the parameter m of the power law is irrelevant. The MHS predicts a non-linear stress-strain curve, which maps the observed behavior better than the MC model, but slightly underestimates the deviatoric stress close to failure, i.e. it reaches the ultimate state more slowly than observed. The MHS model maps well the measured peak volumetric strain, but reaches the peak value later than observed.

One important feature of the MHS model is that it accounts for the stress dependency of the deformation moduli. This is why we examined the model behavior also under radial stresses that are different than that in the test used for the parameter determination (5 MPa). Figures 4 and 5 apply to radial stresses of 2 and 9 MPa, respectively.

Consider the case of a lower radial stress (2 MPa, Fig 4). The MC model greatly overestimates the stress before reaching failure and greatly underestimates the peak volumetric strain. In the case of a higher radial stress (9 MPa, Fig. 5), parameter set 2, which is based upon the secant modulus and maps the observed behavior for the reference radial stress of 5 MPa well (Figure 2), shows the greatest deviation from the test results (both with respect to pre-failure stress and to the volumetric strain). On the other hand, sets 1 and 3, which did not reproduced the behavior in the reference case of 5 MPa well, lead now to acceptable results.

The MHS model better maps the observed behavior over the considered radial stress range, although it may also overestimate the pre-failure stress particularly at lower radial stresses.

5 CONCLUSIONS

The MHS model has four parameters more than the widely used MC model. The parameters have, however, a clear physical meaning and can be determined from the same test results as the MC model. The MHS model predicts the behavior under different stress levels better than the MC model. This may be significant for modeling the conditions around deep tunnels in weak rock, where the minimum principal stress decreases significantly in the vicinity of the opening. The effect of the constitutive law on the response of the ground to tunnel excavation under drained or undrained conditions is currently under investigation.

6 ACKNOWLEDGEMENTS

The authors appreciate the financial support of the Swiss National Science Foundation (project 200021-137888).

7 REFERENCES

Anagnostou, G., Pimentel, E., Cantieni, L. 2008. AlpTransit Gotthard Basistunnel Teilabschnitt Sedrun, Felsmechanische Laborversuche Los 378 Schlussbericht., vol Nr.080109. Inst. für Geotechnik,ETH Zürich.

Benz, T., Wehnert, M. and Vermeer, A. 2008. A Lode Angle Dependent Formulation of the Hardening Soil Model.

Brinkgreve, R. B. J. and Vermeer, P. A. 1997. Plaxis finite element code for soil and rock analysis-Version 7.

Caquot, A. 1934. Equilibre des massifs afrottement interne. Gauthier-Villars, Paris, France.

Duncan, J. M. and Chang, C.-Y. 1970. Nonlinear Analysis of Stress and Strain in Soils. Journal of the Soil Mechanics and Foundations Division. v. 96, no. 5, pp. 1629-1653.

Kovári, K. 1998. Tunnelling in Squeezing Rock. Tunnel. v. 5, no. 98, pp. 12-31.

Rowe, P. 1962. The stress-dilatancy relation for static equilibrium of an assembly of particles in contact. Proceedings of the Royal Society of London. Series A, Mathematical and Physical Sciences. v. 269, no. 1339, pp. 500-527.

Soreide, O.K. 1990. Mixed hardening models for frictional soils. PhD thesis, Norwegian University of Science and Technology (NTNU), Trondheim.